

Experimental realization of light with time separated correlations by rephasing amplified spontaneous emission

Patrick M. Ledingham,^{1,*} William R. Naylor,^{1,†} and Jevon J. Longdell^{1,‡}

¹*Jack Dodd Centre for Photonics and Ultra-Cold Atoms,
Department of Physics, University of Otago, Dunedin, New Zealand.*

(Dated: May 1, 2019)

Amplified spontaneous emission is a common noise source in active optical systems, it is generally seen as being an incoherent noise process. Here we excite an ensemble of rare earth ion dopants in a solid with a π -pulse, resulting in amplified spontaneous emission. The application of a second π -pulse leads to a coherent echo of the amplified spontaneous emission that is correlated in both amplitude and phase. For small optical thicknesses the amplified spontaneous emission and its echo are nonclassically correlated at the 95% confidence level.

PACS numbers: 03.67.-a, 32.80.Qk, 42.50 p, 78.47.jf

Amplified spontaneous emission (ASE) [1] is a ubiquitous phenomena that produces low-temporal coherence light in optical amplifiers. As well as being an unwanted noise process in optical amplifiers [2], and a source of inefficiency in lasers [3], it forms the basis of many useful high brightness, broadband light sources [4]. Recent theoretical work showed that applying rephasing pulses to atoms with long coherence times produces an ‘echo’ of ASE [5]. It was also shown that this rephased amplified spontaneous emission (RASE) is entangled with the ASE provided the optical depth (αl) of the medium is low (< 1).

RASE is attractive in that streams of time separated entangled photons can be created. This is interesting in the context of scaleable, long distance quantum information networking and communication, which requires a quantum repeater [6]. At its heart, a quantum repeater is a source of entangled photons that are separated in time. This way entanglement swapping can entangle two remote stations even though the photons coming from these stations may arrive at different times.

One proposal to realize an elementary link of a quantum repeater using atomic ensembles and linear optics is the Duan-Lukin-Cirac-Zoller (DLCZ) protocol [7]. The DLCZ protocol uses atoms in a lambda configuration. It relies on the fact that every excitation of the spin-wave is accompanied by the absorption of a photon from one of the two coupled optical fields and emission into the other. In the write process the photon is absorbed from the coherent driving field and emitted into the signal field. As a result of this there is a one to one correspondence between the excitations created in the spin-wave and in the signal field. The read process is followed some time later by the write process, where the roles of the two fields are

reversed. This time there is a one to one correspondence between the excitations removed from the spin wave and photons emitted into the signal field. This results in a photon pair source with the photons separated in time. Among the recent achievements in the implementation of the DLCZ protocol are long term storage in a system that produces telecommunication wavelength write photons [8] and the entanglement of four ensembles [9].

RASE has strong parallels to the DLCZ protocol, especially when the upper level of the lambda system can be adiabatically eliminated, meaning the lambda systems can be treated effectively as two level atoms coupled to the signal fields, with the coherent driving field determining the strength of the coupling [5].

In RASE, initially a collection of two level atoms are placed in the excited state, resulting in gain and therefore ASE. For each ASE photon emitted one atom is transferred to the ground state, but like in the case of the DLCZ protocol this de-excitation is coherently spread among the atoms of the ensemble as in a spin-wave. A π -pulse then inverts the ensemble, placing the majority of the atoms in the ground state. The coherence in the atoms produced with the ASE is rephased resulting in collective emission of the RASE. This is different to DLCZ where swapping the control and signal fields means that the effective two level atoms have their ground and excited states reversed. A strong advantage that this gives RASE is that inhomogeneous broadening, rather than limiting the storage, means that the process is temporally multimode with associated improvements for quantum repeater operations [10]. Another way proposed to make a DLCZ-like protocol that is multimode involves structuring the optical inhomogeneous broadening [11] in a similar way to atomic frequency comb memories [12]. In the case of RASE in Tm^{3+} :YAG considered here, the inhomogeneous broadening is approximately 30 GHz, meaning that practically the bandwidth of the process is only limited by the bandwidth of the exciting and rephasing π -pulses. This is because, unlike the majority of quantum memory techniques using rare earths, RASE doesn't require spectral tailoring.

*Present address: ICFO-Institut de Ciències Fotoniques, Av. Carl Friedrich Gauss 3, 08860 Castelldefels (Barcelona), Spain

†Present address: Department of Physics, Norwegian University of Science and Technology, N-7491 Trondheim, Norway

‡Electronic address: jevon.longdell@otago.ac.nz

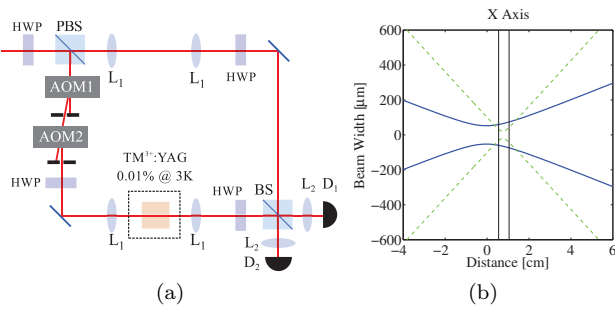


FIG. 1: (Color online) (a) Experimental setup. Laser beam passes through a polarizing beamsplitter (PBS). The probe arm is steered through two Acousto-Optic Modulators (AOM) for pulse generation, then steered toward the cryogenic $\text{Tm}^{3+}:\text{YAG}$. The signal is then combined with the local oscillator (LO) on a non-polarizing beamsplitter (BS) and sent to a balanced pair of detectors. The two AOMs introduce a net frequency shift of 10.7 MHz between the light used to drive the $\text{Tm}^{3+}:\text{YAG}$ and the local oscillator. The waveplates ensure that this driving light and the local oscillator have the same polarisation at the BS. (b) In order to only collect light from atoms that had seen close to π -pulses, we intentionally had the interferometer mis-modematched. The beam diameter of the exciting light (blue solid curves) had larger diameter in the crystal (parallel lines) than would be the case for the modematched beam (green dashed curves).

Another route to a quantum repeater is to use a more standard parametric downconversion source of photon pairs and then store one of these in a quantum memory based on rare earth ion dopants. This has recently been demonstrated [13, 14]. This approach holds great promise because of the storage time [15], bandwidths [16], and efficiencies [17, 18] that have recently been achieved. Using RASE rather than downconversion for the sources in such experiments would greatly simplify the experiments, naturally providing sources with the appropriate brightness, wavelength and bandwidths.

Here we report on correlated, time separated, optical fields using RASE in cooled thulium doped (0.1%) yttrium aluminum garnet ($\text{Tm}^{3+}:\text{YAG}$). In the experiments we applied two π -pulses to an inhomogeneously broadened ensemble of two level atoms. The first π -pulse inverts the population of a portion of the inhomogeneously broadened line resulting in ASE. A second π -pulse places these atoms down near to the ground state, rephasing any coherence in the sample that is produced by ASE to form RASE. Shot-noise limited balanced heterodyne detection is used to characterize the ASE and the RASE by measuring variances of the light quadratures \hat{x} and \hat{p} . This was chosen over homodyne because of the need for the detection system to recover quickly after being saturated by the π -pulses.

The experimental setup used is shown in Fig. 1. Additional experimental details are found in Appendix A. When trying to apply optical pulses with accurate pulse areas the transverse variation in intensity of a Gaussian

mode is problematic. One approach is to image the light from the optical spot on the crystal onto an aperture [19] in such a way that only light from ions near the center of the spot contributes to the detected signal. The approach we take here is similar except rather than using an aperture we use the spatial filtering properties of heterodyne detection, to detect in a mode that has a smaller diameter at the sample than the driving field. The modes are illustrated in Fig. 1(b).

A benefit of using $\text{Tm}^{3+}:\text{YAG}$ is that, at zero magnetic field, it lacks a long term spectral holeburning mechanism. A long term spectral holeburning mechanism is undesirable because it generally leads to inadvertent structure being prepared in the inhomogeneous absorption profile. This structure, even with very low absorption contrast, leads to optical free-induction decays (FIDs) which mask the ASE and RASE fields. At zero magnetic field there is no structure for the ground and excited states we are using. The longest lived spectral holeburning mechanism is due to the metastable $^3\text{F}_4$ level which has a lifetime of ~ 10 ms [20]. The 10 Hz repetition rate used for the experiment ensures that this level was effectively emptied between shots. Another way to avoid the random FIDs associated with spectral holeburning is the four level scheme of [21].

Figure 2 shows the results of experiments carried out on a physically and optically thick sample (20 mm, $al = 3.2$). In this large gain regime it is expected that any correlations will be classical [5] but large signals improve the signal to noise ratios. Figure 2(a) shows the pulse sequence used as well as the variance of both quadratures as a function of time. The first pulse is used to measure the phase of the interferometer, it contains enough photons to make a good measurement of the phase but doesn't significantly drive the ions. The length of the π -pulse is 1.6 μs . An echo (labeled 'Echo' in Fig. 2(a)) is formed due to the pulse π_2 rephasing the coherence inadvertently caused by π_1 .

There is a distinct increase of the variance after application of π_1 which is due to amplified spontaneous emission. The ASE decay time is 378 μs . This rules out the possibility we are instead seeing FIDs, as they would have decayed on timescales at least as short as the coherence time, T_2 . Using a two pulse photon echo sequence, the coherence time is measured to be 13 μs . The second π -pulse, π_2 , then rephases the atomic state left in the crystal by the ASE and so the corresponding field should have a decreased variance relative to the ASE. It is seen that indeed the variance has decreased in the RASE time window, however the timescales here are comparable to the ASE lifetime so the resulting decrease could be from the natural excited state population decay. To confirm the effect of π_2 , the spectral power is extracted from the indicated temporal regions of Fig. 2(a) and plotted in the left panel of Fig. 2(b). The spectra are normalized to the vacuum case. The ASE spectrum shows a narrow feature of noise characteristic of the narrow-band gain created by the inverting π -pulse. The width of this feature is about

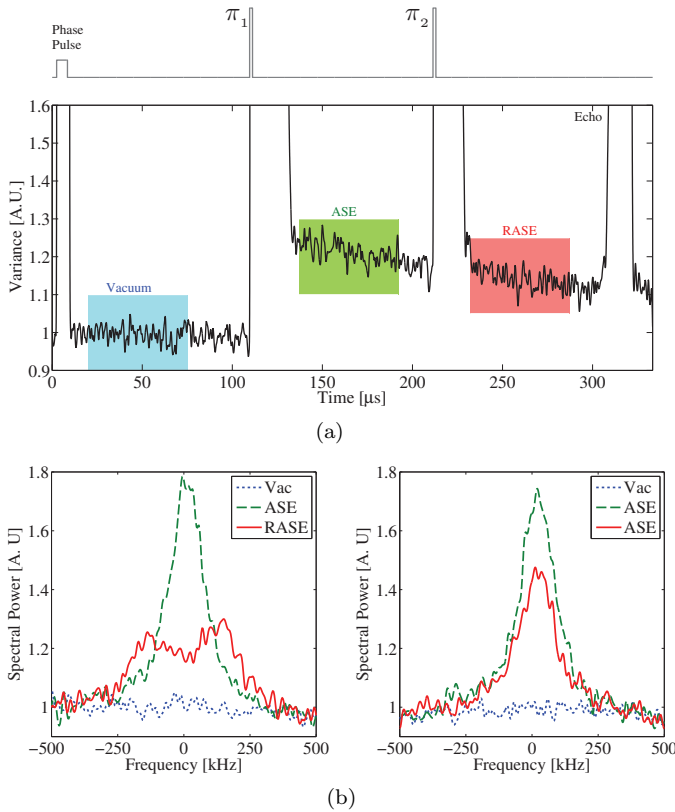


FIG. 2: (Color online) (a) Measured total variance of the quadrature measurements as a function of time for the optically thick sample. (b) The spectral power of the three regions for two different cases. Left panel: Spectra for the pulse sequence seen in (a). Right panel: Spectra for the same time windows but with π_2 removed.

150 kHz, comparable to the Fourier width of the π -pulse. The RASE spectrum shows a distinct decrease on resonance with the driving laser. The effect is accentuated when compared to the case when π_2 is removed from the sequence (right panel of Fig. 2(b)). This suggests that the second π -pulse has the expected effect of driving the remaining excited ions back to the ground state.

It is noted that the measured length of the transmitted π -pulse has increased significantly, from 1.6 μs to near 30 μs . This is because of two reasons. Firstly, the detection system saturates the detection system and it has a finite recovery time. Secondly, due to the area theorem [19, 22], a π -pulse remains a π -pulse while propagating through an absorbing medium, resulting in the pulse lengthening as the intensity decreases. This will effect the bandwidth of the ASE and RASE, so that the measured π -pulse provides an upper bound on the ASE and RASE bandwidth.

The ASE and RASE fields for this optically thick sample are significantly smaller that would be expected based on the optical depth ($\text{ASE} \propto \exp[\alpha l]$, $\text{RASE} \propto \sinh^2[\alpha l/2]$ [5]). This was ascribed to the difficulties in inverting the ions in physically and opti-

cally thick samples. Measurements of gain through the sample after the first π -pulse support this. Subsequent experiments were carried out with thinner samples which reduced this problem.

Figure 3(a) shows the magnitude of the cross correlation between the ASE and RASE fields for the three different optical depths (0.25, 0.47 and 0.78) and for the case where the crystal is warmed to ~ 40 K. At such warm temperatures, any atomic coherence is lost on nanosecond timescales. The cross correlation is obtained for each individual shot and the mean and then magnitude is plotted. There is a distinct correlation peak that appears above the warm case for all three cold cases clearly confirming a time separated correlation between the ASE and RASE fields. As expected when the optical depth decreases the ASE and RASE fields become weaker and the magnitude of the correlation is reduced.

To test the nonclassical nature of this time separated correlation, we invoke the inseparability criterion for continuous variable states created by Duan et al. [24]. One can express a maximally entangled state as a co-eigenstate of a pair of EPR type operators $\hat{u} = \sqrt{b} \hat{x}_1 + \sqrt{1-b} \hat{x}_2$ and $\hat{v} = \sqrt{b} \hat{p}_1 - \sqrt{1-b} \hat{p}_2$, where $b \in [0, 1]$, \hat{x} and \hat{p} are the light quadratures and the subscript 1 (2) indicates the ASE (RASE) field. For any separable state ρ , the total variance of \hat{u} and \hat{v} satisfies

$$\langle (\Delta \hat{u})^2 \rangle + \langle (\Delta \hat{v})^2 \rangle \geq 2. \quad (1)$$

For inseparable states, the total variance is bound from below by zero.

By appropriately windowing and then integrating the heterodyne measurement record, values for \hat{x} and \hat{p} for a temporal mode in both the ASE and RASE regions were obtained. Heterodyne detection gives simultaneous and noisy measurements for both quadrature amplitudes,

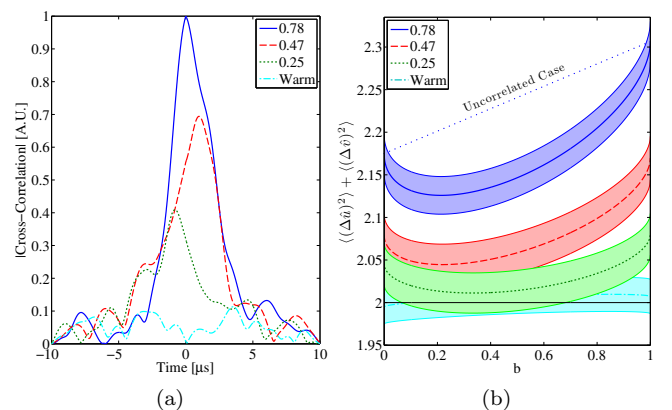


FIG. 3: (Color online) (a) The cross correlation function between the ASE and RASE fields for three different optical depths 0.25, 0.47, 0.78 and the case where the sample is warmed to 40 K. (b) The inseparability criterion for the same cases as (a). The uncorrelated case is shown for $\alpha l = 0.78$. The shaded areas correspond to a confidence interval of 95% and are calculated as in [23].

as opposed to homodyne detection giving good measurements of just one. However as is discussed in Appendix B, we can still use Eq. 1 as our inseparability criterion.

Figure 3(b) shows the inseparability criterion versus b for the optically thin cases of 0.25, 0.47 and 0.78. For $b = 1$ the variance is purely the ASE field and for $b = 0$ the variance is purely the RASE field. An indication of how strongly the fields are correlated is the amount the curve dips below the uncorrelated case (straight line between the ASE and RASE values). It is seen that for the $al = 0.78$ case there is a prominent dip for low b . As the optical depth is reduced, this dip becomes less pronounced, owing to the decrease in photons. This behavior is also seen in the cross correlation measurements. The temporal mode-functions chosen were square and are described in Appendix A.

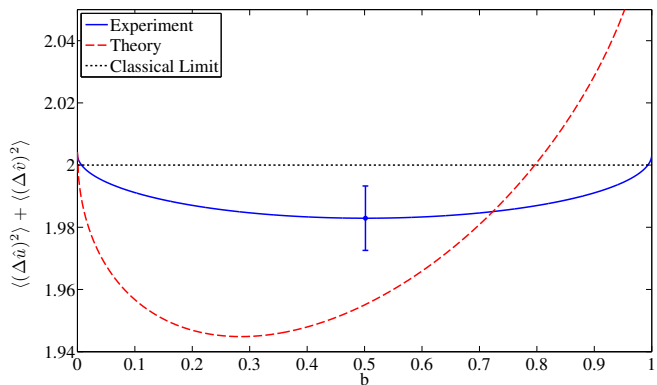


FIG. 4: (Color online) Inseparability criterion for the ultra-thin case of optical depth 0.046 (solid blue line). The dashed line shows what can be expected theoretically in the ideal case of perfect π -pulses and no dephasing. The error bar is 1σ centered on the lowest point of the dip. The confidence level that this point is below the classical bound is 95.15%

Figure 4 shows results for a very optically thin sample (0.5 mm, $al = 0.046$). The time between π_1 and π_2 was $40 \mu\text{s}$, the temporal mode functions were Gaussian with a width of $2.5 \mu\text{s}$ placed $10.5 \mu\text{s}$ either side of π_2 . Owing to the low optical depth and thus less temporal broadening of the π -pulse under propagation, the RASE and ASE windows are allowed to be moved closer to π_2 . To obtain quadrature variances, 22 000 shots were acquired in 44 batches of 500. Each batch had the cryo-cooler off to reduce laser noise and between the batches the cryo-cooler was restarted to cool the sample back to 3 K. The off time of the cryo-cooler was chosen such that the T_2 was not significantly affected. The batches were taken over a period of 2 days. Figure 4 shows the inseparability criterion calculated from the measured ASE and RASE fields. Here, the inseparability curve clearly dips below the classical bound. Furthermore, at the lowest point in the dip ($b = 0.5015$), the separability criterion is violated to a confidence level of 95.15%. Shown also in Fig. 4 is the theoretical curve expected from using a heterodyne detector and analytic expressions for the ASE and RASE

fields obtained from [5]. Due to the use of imperfect π -pulses to generate and rephase the fields, the measured amount of ASE and RASE, the level of inseparability and the position of the minimum are in disagreement with theory.

While Fig. 3 shows multimode correlations between the ASE and RASE fields, the experiment in its current form is unable to demonstrate multimode entanglement. There were three experimental constraints on the timescales and bandwidth of operation. These were the coherence lifetime T_2 , the detection recovery time and the available laser power (and therefore the bandwidth of the π -pulses). These constraints opened a large enough time window to demonstrate nonclassicality with one temporal mode.

The outlook of rephased amplified spontaneous emission as a broadband entangler of photons is promising. Nonclassical correlations were demonstrated in this work but variations of this experiment can be implemented. Changing to a material with a greater coherence time, and thus allowing for multimode demonstrations, is a possibility. $\text{Tm}^{3+}:\text{YAG}$ was chosen for its ineffective holeburning feature so as to avoid FID phenomena resulting from holeburnt features. Changing to a material such as $\text{Pr}^{3+}:\text{Y}_2\text{SiO}_5$ will see an increase in coherence time and FID phenomena can be avoided by phase-matching [25] or a four level echo scheme [21]. The four level scheme has the advantage that between the ASE and RASE coherence is stored in the spin states, potentially allowing longer storage times [15]. Operation at telecommunication wavelengths is possible using erbium dopants where the potential for long lived spin coherences has recently been identified [26]. The nonclassicality shown here is small and on the edge of statistical significance, even in the ideal two level atom case RASE does not achieve perfect entanglement. This can be seen as a consequence of a fixed optical depth. Ideally weak interaction with the light is required when generating the ASE, this means that there is on average a small number of photons per spatio-temporal mode. Then strong interaction with the light is required to efficiently retrieve the RASE. Beavan et al.'s four level scheme [21], Raman transitions with changing coupling strengths, and Q-switched cavities [27] are all ways of achieving changes in the effective optical depth.

In conclusion we have demonstrated the generation of ASE and RASE fields from a cryogenically cooled $\text{Tm}^{3+}:\text{YAG}$ crystal for different optical depths. The effect of the second π -pulse (π_2) is clearly seen in the spectrum of the optically thick case. Clear time separated correlation peaks are observed between the ASE and RASE fields for optical depths ranging from 0.25 to 0.78. For an optical depth of 0.046, the ASE and RASE fields were entangled at the 95% confidence level.

We note that a similar work demonstrating time separated correlations in a praseodymium doped crystal has been performed independently [28].

This research was funded by the New Zealand Founda-

tion for Research Science and Technology under Contract No. NERF-UOOX0703.

Appendix A: Experimental details

An external cavity diode laser was locked to a spectral hole in a second Tm:YAG crystal using a hybrid technique involving optical and electronic locking [29]. The phase of the laser was stable, with respect to coherent processes (such as photon echoes) in the thulium ions for hundreds of microseconds. The Tm³⁺:YAG crystal (Scientific Materials Corp.) was held at 3 K in a pulse tube cryo-cooler, and measurements were taken in batches after the cryo-cooler had been turned off but before the sample had warmed up enough to affect the optical T_2 . The crystal was cut such that the light propagated along the $\langle 1\bar{1}0 \rangle$ direction. The two level transition used was ${}^3\text{H}_6 \leftrightarrow {}^3\text{H}_4$ with a wavelength of 793.156 nm in air. A lens (L_1) of 100mm is used to focus the beam at the sample, the beam waist being 53 μm . Rabi frequencies of $\Omega/(2\pi) = 2$ MHz were achieved driving powers of 10 mW.

The photodetectors were produced in house based on a design by Gray et al.[30] but using AD829 op-amps. The beat notes are subtracted using a RF splitter/combiner, amplified with an amplifier that quickly recovers from saturation (Stanford SR445A), bandpass filtered around 10.7 MHz with minicircuits components and then digitized. They are then demodulated using software to give two quadrature amplitudes as a function of time.

For the results of Figure 2(a) the temporal distance between the two π pulses is 100 μs , the windows of interest are 55 μs wide and are centered 47.5 μs either side of π_2 . To obtain the variance, the pulse sequence is applied 2500 times at a repetition rate of 10 Hz. The 100 ms delay between shots allows enough time for total population decay between shots. There are three regions of interest labeled as Vacuum, ASE and RASE. The trace has been normalized to the vacuum window. The π pulse length is 1.6 μs . The coherence time is measured to be 13 μs using a two pulse photon echo sequence. A phase pulse is

placed at a time of 100 μs before π_1 , an order of magnitude larger than the coherence time measured. This ensures that an echo of this phase pulse does not interfere with the ASE or RASE windows of interest. Moreover, the echo would appear at the same temporal location as π_2 . The phase pulse is also weak such that the detection system is not saturated. It is noted that there is an echo of π_1 rephased by π_2 .

Referring to Figure 3(a), the characteristic timescales used to generate the ASE and RASE fields for this case are as follows : 60 μs between π_1 and π_2 , the windows are 10 μs wide centered 30 μs either side of π_2 . It is noted that the coherence time for this case is 23 μs due to the crystal being seemingly colder. Due to the reduction in the magnitude of the ASE and RASE fields, this pulse sequence is applied 20×10^3 , 14.5×10^3 and 18.5×10^3 times at a 10 Hz repetition rate for the optical depth cases of 0.25, 0.47 and 0.78 respectively, to obtain statistics.

Appendix B: Measuring the Inseparability Criterion with a Heterodyne Detector

Here we show that the inseparability criterion of Duan et al. [24] has the same bound for heterodyne detection as for homodyne detection. Moreover, it is shown that a heterodyne detector can measure the nonclassical correlation albeit less sensitively.

Heterodyne detection can be described as ‘noisy’ homodyne detection, simultaneously measuring both light quadratures . When measuring the quadrature \hat{x}_i with a heterodyne detector, one measures

$$\hat{x}_i \rightarrow \frac{\hat{x}_i + \widehat{\text{vac}}_i}{\sqrt{2}},$$

where $i = 1$ or 2 and $\widehat{\text{vac}}_i$ is the vacuum that enters the unused port of the 50:50 beamsplitter or equivalently the vacuum noise at $-\omega$ where ω is the heterodyning frequency. For the inseparability criterion given by Equation 1 (in paper), the variance of the operator \hat{u} becomes,

$$\begin{aligned} \text{var}(u) &\rightarrow b \left\langle \left(\frac{\hat{x}_1 + \widehat{\text{vac}}_1}{\sqrt{2}} \right)^2 \right\rangle + (1-b) \left\langle \left(\frac{\hat{x}_2 + \widehat{\text{vac}}_2}{\sqrt{2}} \right)^2 \right\rangle + 2\sqrt{b(1-b)} \left\langle \left(\frac{\hat{x}_1 + \widehat{\text{vac}}_1}{\sqrt{2}} \right) \left(\frac{\hat{x}_2 + \widehat{\text{vac}}_2}{\sqrt{2}} \right) \right\rangle \\ &= \frac{b}{2} \left(\langle \hat{x}_1^2 \rangle + \langle \widehat{\text{vac}}_1^2 \rangle + \langle \hat{x}_1 \widehat{\text{vac}}_1 \rangle + \langle \widehat{\text{vac}}_1 \hat{x}_1 \rangle \right) + \frac{1-b}{2} \left(\langle \hat{x}_2^2 \rangle + \langle \widehat{\text{vac}}_2^2 \rangle + \langle \hat{x}_2 \widehat{\text{vac}}_2 \rangle + \langle \widehat{\text{vac}}_2 \hat{x}_2 \rangle \right) \\ &\quad + \sqrt{b(1-b)} \left(\langle \hat{x}_1 \hat{x}_2 \rangle + \langle \widehat{\text{vac}}_1 \widehat{\text{vac}}_2 \rangle + \langle \hat{x}_1 \widehat{\text{vac}}_2 \rangle + \langle \widehat{\text{vac}}_1 \hat{x}_2 \rangle \right). \end{aligned}$$

Since the variance of the vacuum is 1 and that the covariance terms between \hat{x} and the vacuum equate to zero then,

$$\text{var}(u) = \frac{b}{2} (\langle \hat{x}_1^2 \rangle + 1) + \frac{1-b}{2} (\langle \hat{x}_2^2 \rangle + 1) + \sqrt{b(1-b)} (\langle \hat{x}_1 \hat{x}_2 \rangle)$$

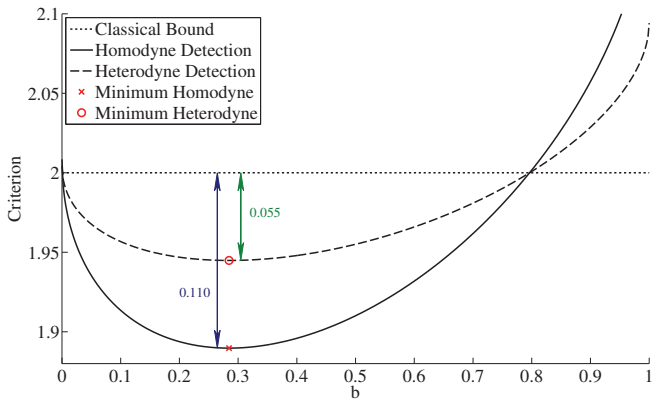


FIG. 5: Inseparability criterion for homodyne (solid line) and heterodyne (dashed line) detection. The classical bound (dotted line) is the same for both cases (see text). The curves are plotted for the experimentally relevant case of $\alpha l = 0.046$. The cross and circle indicate the minimum of the curve for homodyne and heterodyne detection respectively. Arrows indicate the ‘dip’ below the classical bound for the minima. Heterodyne detection results in a factor of 2 less ‘dip’ compared to homodyne detection. This factor of 2 is the case for any point on the curve dipping below the classical bound.

For the case where the ASE and RASE fields (\hat{x}_1 and \hat{x}_2) are the vacuum, then the variance measured for the operator \hat{u} is 1. A similar treatment to above can be done to the \hat{p} quadrature resulting in the variance of the \hat{v} operator to be 1 for the case of vacuum ASE and RASE fields. The result is that the classical bound for violating the inseparability criterion using a heterodyne detector is $\text{var}(\hat{u}) + \text{var}(\hat{v}) = 2$.

When comparing the above equation to the homodyne case, a factor of 2 is lost in front of the covariance term $\langle \hat{x}_1 \hat{x}_2 \rangle$. Hence, the correlation between the ASE and RASE fields (or equivalently, the ‘dip’ below the classical bound) is reduced by a factor of 2 when using a heterodyne detector. Figure 5 show the theoretical inseparability curves for homodyne and heterodyne detection for the experimentally relevant case of $\alpha l = 0.046$.

-
- [1] L. Allen and G. I. Peters, Phys. Rev. A **8**, 2031 (1973).
[2] C. Henry, J. Lightw. Technol. **4**, 288 (1986).
[3] N. Barnes and B. Walsh, IEEE J. Quantum Electron. **35**, 101 (1999).
[4] P. Wysocki, M. Digonnet, B. Kim, and H. Shaw, J. Lightw. Technol. **12**, 550 (1994).
[5] P. M. Ledingham, W. R. Naylor, J. J. Longdell, S. E. Beavan, and M. J. Sellars, Phys. Rev. A **81**, 012301 (2010).
[6] H.-J. Briegel, W. Dur, J. I. Cirac, and P. Zoller, Phys. Rev. Lett. **81**, 5932 (1998).
[7] L. M. Duan, M. D. Lukin, J. I. Cirac, and P. Zoller, Nature **414**, 413 (2001).
[8] Y. O. Dudin, A. G. Radnaev, R. Zhao, J. Z. Blumoff, T. A. B. Kennedy, and A. Kuzmich, Phys. Rev. Lett. **105**, 260502 (2010).
[9] K. S. Choi, A. Goban, S. B. Papp, S. J. van Enk, and H. J. Kimble, Nature **468**, 412 (2010).
[10] C. Simon, H. de Riedmatten, M. Afzelius, N. Sangouard, H. Zbinden, and N. Gisin, Phys. Rev. Lett. **98**, 190503 (2007).
[11] P. Sekatski, N. Sangouard, N. Gisin, H. de Riedmatten, and M. Afzelius, Phys. Rev. A **83**, 053840 (2011).
[12] M. Afzelius, C. Simon, H. de Riedmatten, and N. Gisin, Phys. Rev. A **79**, 052329 (2009).
[13] C. Clausen, I. Usmani, F. Bussières, N. Sangouard, M. Afzelius, H. de Riedmatten, and N. Gisin, Nature **469**, 508 (2011).
[14] E. Saglamyurek, N. Sinclair, J. Jin, J. A. Slater, D. Oblak, F. Bussières, M. George, R. Ricken, W. Sohler, and W. Tittel, Nature **469**, 512 (2011).
[15] J. J. Longdell, E. Fraval, M. J. Sellars, and N. B. Manson, Phys. Rev. Lett. **95**, 063601 (2005).
[16] I. Usmani, M. Afzelius, H. Riedmatten, N. Gisin, and H. de Riedmatten, Nature Comms. **1**, 12 (2010).
[17] M. P. Hedges, J. J. Longdell, Y. Li, and M. J. Sellars, Nature **465**, 1052 (2010).
[18] T. Chanelière, J. Ruggiero, M. Bonarota, M. Afzelius, and J. L. Gouët, New J. Phys. **12**, 023025 (2010).
[19] J. Ruggiero, T. Chanelière, and J.-L. Le Gouët, J. Opt. Soc. Am. B **27**, 32 (2009).
[20] R. M. Macfarlane, Opt. Lett. **18**, 829 (1993).
[21] S. E. Beavan, P. M. Ledingham, J. J. Longdell, and M. J. Sellars, Opt. Lett. **36**, 1272 (2011).
[22] E. L. Hahn, N. S. Shiren, and S. L. McCall, Phys. Lett. **37**, 265 (1971).
[23] Y. Bar-Shalom, X. R. Li, and T. Kirubarajan, *Estimation with Applications to Tracking and Navigation* (Wiley-Interscience, 2001), ISBN 047141655X.
[24] L.-M. Duan, J. I. Cirac, P. Zoller, and E. S. Polzik, Phys. Rev. Lett. **85**, 5643 (2000).
[25] V. Damon, M. Bonarota, A. Louchet-Chauvet, T. Chanelière, and J.-L. Le Gout, New J. Phys. **13**, 093031 (2011).
[26] D. L. McAuslan, J. G. Bartholomew, M. J. Sellars, and J. J. Longdell, Phys. Rev. A **85**, 032339 (2012).
[27] In preparation.
[28] S. E. Beavan, M. P. Hedges, and M. J. Sellars, in preparation.
[29] W. G. Farr, J. W. Tay, P. M. Ledingham, D. Korystov, and J. J. Longdell, arXiv.org (2010).
[30] M. B. Gray, D. A. Shaddock, C. C. Harb, and H.-A. Bachor, Rev. Sci. Instrum. **69**, 3755 (1998).